Characterization of an active metasurface using terahertz ellipsometry

Nicholas Karl, Martin S. Heimbeck, Henry O. Everitt, Hou-Tong Chen, Antoinette J. Taylor, Igal Brener, Alexander Benz, John L. Reno, Rajind Mendis, and Daniel M. Mittleman

Citation: Appl. Phys. Lett. **111**, 191101 (2017);
View online: https://doi.org/10.1063/1.5004194
View Table of Contents: http://aip.scitation.org/toc/apl/111/19
Published by the American Institute of Physics

Characterization of an active metasurface using terahertz ellipsometry

Nicholas Karl,[1] Martin S. Heimbeck,[2] Henry O. Everitt,[2] Hou-Tong Chen,[3] Antoinette J. Taylor,[3] Igal Brener,[4] Alexander Benz,[4] John L. Reno,[4] Rajind Mendis,[1] and Daniel M. Mittleman[1]

[1]*School of Engineering, Brown University, 184 Hope St., Providence, Rhode Island 02912, USA*
[2]*U.S. Army AMRDEC, Redstone Arsenal, Huntsville, Alabama 35808, USA*
[3]*Center for Integrated Nanotechnologies, Los Alamos National Laboratory, Los Alamos, New Mexico 87545, USA*
[4]*Center for Integrated Nanotechnologies, Sandia National Laboratories, Albuquerque, New Mexico 87185, USA*

(Received 11 September 2017; accepted 19 October 2017; published online 6 November 2017)

Switchable metasurfaces fabricated on a doped epi-layer have become an important platform for developing techniques to control terahertz (THz) radiation, as a DC bias can modulate the transmission characteristics of the metasurface. To model and understand this performance in new device configurations accurately, a quantitative understanding of the bias-dependent surface characteristics is required. We perform THz variable angle spectroscopic ellipsometry on a switchable metasurface as a function of DC bias. By comparing these data with numerical simulations, we extract a model for the response of the metasurface at any bias value. Using this model, we predict a giant bias-induced phase modulation in a guided wave configuration. These predictions are in qualitative agreement with our measurements, offering a route to efficient modulation of THz signals. *Published by AIP Publishing*. https://doi.org/10.1063/1.5004194

The possibility of using terahertz (THz) frequencies for wireless communications is attracting much research interest.[1,2] One of the key challenges for THz devices is phase modulation. A low-loss high-speed phase modulator would be valuable in numerous applications, such as for advanced data modulation[3] or for electrically driven beam steering.[4] Many different approaches to modulation have been discussed,[5–7] with a recent focus on active metamaterial-based structures.[8] These metamaterials are planar structures (i.e., metasurfaces), with active elements integrated into the layer[9,10] or with the meta-elements fabricated on a lightly doped epilayer with active electrical control of the carrier density via the formation of a Schottky contact.[11–15] In most cases, however, the magnitude of the phase modulation is well below 2π, limited by the effective interaction length of a free-space propagating wave normally incident on a two-dimensional structure.

One intriguing alternative is to use a guided wave geometry, in which the THz electromagnetic wave propagates parallel to the metasurface. This approach would enable a dramatic increase in the effective interaction length between the THz wave and the metasurface. In combination with actively tunable meta-elements, this idea offers a promising route to high-contrast electrical phase modulation. Moreover, this guided wave geometry is compatible with pixelation of the metasurface for versatile wavefront engineering.[12–14] Previous studies have considered surface plasmon waves propagating on passive THz metasurfaces.[16,17] However, active metasurfaces have so far not been studied in a waveguide geometry. Indeed, the extent to which electrical modulation changes the surface parameters has not yet been quantified with sufficient accuracy to model a dielectric slab waveguide structure in which the modulated surface forms one of the dielectric-air boundaries.[18,19] Active metasurface devices have a large design space to explore, and metamaterial scattering element design is a rich field.[20] Yet, predicting the performance of the active nature of such devices is an open question, making optimization of practical devices difficult, especially if the fundamental switching performance is not well characterized.

Here, we report the results of characterization measurements on a switchable metasurface, performed using spectroscopic THz ellipsometry.[21,22] By optimizing the concurrence between the experimental data and a model prediction, we develop a relation between the external input of an active metasurface (i.e., the applied switching voltage) and the material properties of the substrate. Based on the results of this analysis, we build a numerical model to predict the phase modulation performance of the metasurface in a dielectric slab waveguide geometry. This prediction agrees qualitatively with our experimental results and points the way towards the development of a high-speed, low-loss, and high-contrast THz phase modulator.

Our metasurface device is comprised of electric split-ring resonator (eSRR) scattering elements on an intrinsic GaAs substrate with a 1-μm-thick *n*-doped epilayer (carrier density $\sim 2 \times 10^{16}\,\mathrm{cm}^{-3}$). The eSRR elements, shown in Fig. 1(a), feature a strong resonance at 400 GHz when illuminated at normal incidence[13] and are interconnected with metallic wires, making a Schottky contact with a pad for the external bias, as shown in Fig. 1(b). The mechanism behind the active control of the metasurface has been described previously: the excess electrons in the *n*-doped epilayer effectively short the capacitive split-ring gap and damp the resonant response.[11,13] A DC reverse bias depletes the charges in the substrate underneath the eSRR, reducing the conductivity and restoring the capacitive response and the THz resonance. Typically, the magnitude of the phase modulation of such a device (i.e., the difference in the phase between the state where the maximum voltage is applied and where no voltage is applied) is about

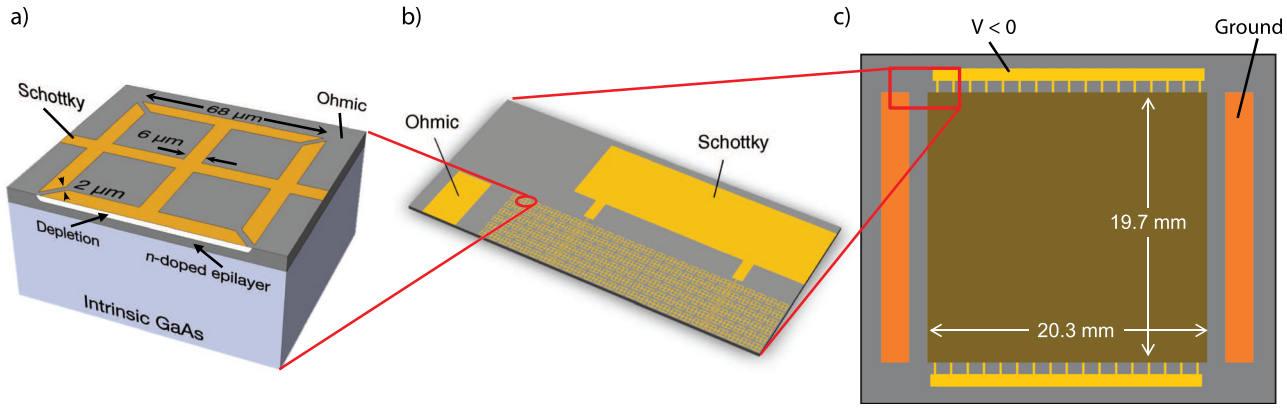

FIG. 1. (a) Illustration of the metasurface unit cell and substrate, showing an individual eSRR element. The dark gray substrate layer represents the higher carrier density in the *n*-doped GaAs epilayer, and the white region beneath the metal Schottky structure indicates the depletion in the epilayer upon a reverse voltage bias. (b) Schematic showing how the eSRR elements in (a) are tiled to form the metasurface array. The entire array is interconnected making up the Schottky gate; one of each of the Ohmic and Schottky pads is shown. (c) Illustration of the metasurface device. The dark gold region indicates the metasurface array, controlled by the reverse voltage bias applied between the Schottky pads (yellow) and the Ohmic contacts (orange).

0.5 rad in a normal-incidence transmission geometry,[8] which, although impressive for a 2D structure, is still not sufficient for, e.g., wide-angle beam steering or advanced data modulation schemes.

To understand the voltage-driven response of our metasurface device in detail, we employ THz ellipsometry. Ellipsometry is a sensitive technique for surface characterization because it measures the polarization and relative phase change induced in a polarized beam after reflection from the sample and is thereby largely insensitive to amplitude noise in the THz source.[21,22] The measured quantities are Ψ, the amplitude ratio between the *s* and *p* polarization components, and Δ, the phase difference between the polarization components. Ψ and Δ are directly related to the Fresnel reflection coefficients for the *s* and *p* linear polarization states, according to $R_s/R_p = \tan\Psi e^{i\Delta}$. In order to derive useful results from an ellipsometry measurement, we need to solve an inverse problem, where we model the physical system which has some unknown parameters and seek the best match between our prediction and the experiment.[23] We use a frequency domain variable angle spectroscopic ellipsometry (VASE) setup,[21] which uses a backward-wave oscillator (BWO) with Schottky-diode multipliers to generate continuously tunable radiation between 330 and 515 GHz. The system is a rotating-polarizer rotating-compensator ellipsometer, having a fixed analyzer. Detection is performed using a Golay cell. Rotation stages are used for angle of incidence control, where the sample holder and detection subassembly rotate in tandem during data collection. We acquire data at angles of incidence from 30° to 60° in 10° increments, over the full bandwidth of the BWO source. At each angle of incidence, we measure the response for 6 different voltages applied to the metasurface.

Figure 2 shows a typical dataset. This displays Ψ and Δ versus frequency, measured at an incidence angle of 30°. The slow oscillations in both Ψ and Δ originate from Fabry-Pérot interference due to multiple reflections in the 650-μm-thick GaAs substrate. On top of this oscillating background, we readily observe the effect of the applied voltage bias on the surface characteristics which are probed through this measurement. We note that this surface tuning is not limited to the frequency region near the eSRR resonance (at 400 GHz); indeed, we see a significant voltage dependence in Ψ and Δ across the entire measured frequency range. This indicates that the applied bias is tuning a coupled amplitude and phase modulation between the *s* and *p* reflection coefficients, as anticipated.[8]

For the analysis of the measured Ψ and Δ data, we build a model using finite element method (FEM) simulations, with the dimensions given in Fig. 1. The unit cell (Floquet) boundary condition was used to describe the array with

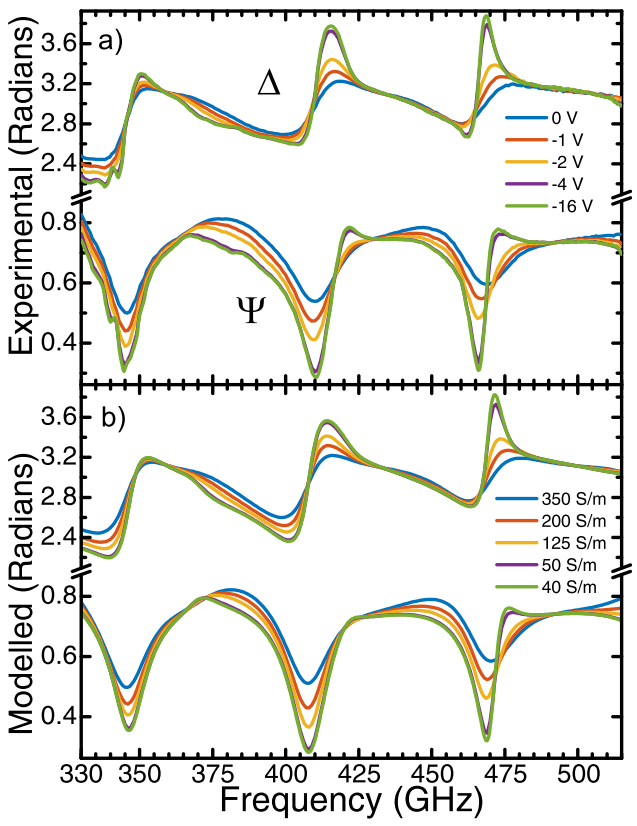

FIG. 2. (a) Experimental metasurface ellipsometry parameter spectra for different values of applied reverse voltage bias at an angle of incidence of 30°. Sharp features emerge on top of the Fabry-Pérot interference as the external bias increases. (b) Modelled Ψ and Δ spectra at an angle of incidence of 30° for the best-fit epilayer conductivity parameters that correspond to the voltages in (a).

88 μm periodicity. Vacuum regions at the input and output for excitation and absorption in free space had a thickness of 200 μm. Adaptive mesh refinement was used with the final structure having ~100k elements. We account for the applied DC bias by varying the simulated conductivity of the top 1 μm region of GaAs (corresponding to the epilayer thickness). This choice is useful because it is intuitive and simple; a relation to epilayer conductivity can be used effectively in the design of active devices. Obviously, the conductivity in the real device is not spatially uniform at any given DC voltage, as the carrier density must vary with the distance from the metal-semiconductor contact. However, we have confirmed that a more complicated model (than what is presented here) which attempts to account for this non-uniformity does not significantly improve the agreement between the simulations and experiments. The results of simulations for Ψ and Δ are shown in Fig. 2(b) for the same situation as the experimental results in Fig. 2(a); the correspondence is remarkably good. Figure 3 shows data at other angles of incidence, directly comparing the numerical results with the measured data, and each voltage is compared with the corresponding modelled conductivity as seen in Fig. 2. The agreement is satisfactory at all angles. We note that the agreement becomes slightly worse at lower frequencies, possibly due to the fact that at oblique illumination angles, the elliptical spot size of the THz beam approaches the size of the sample at low frequencies.

By optimizing results such as those shown in Figs. 2 and 3, we can extract the epilayer conductivity parameter for each value of the DC bias studied in the experiments. We use a regression analysis by minimizing the mean squared error between the measured and simulated spectra. These results, shown in Fig. 4 (data points), show that at low reverse bias, the conductivity drops quickly but then saturates at higher voltage. This saturation is consistent with previous observations of the voltage-induced change in the normal-incidence THz transmission on similar devices.[8,11,13] The best fit conductivity for zero volts, 350 S/m, is also in

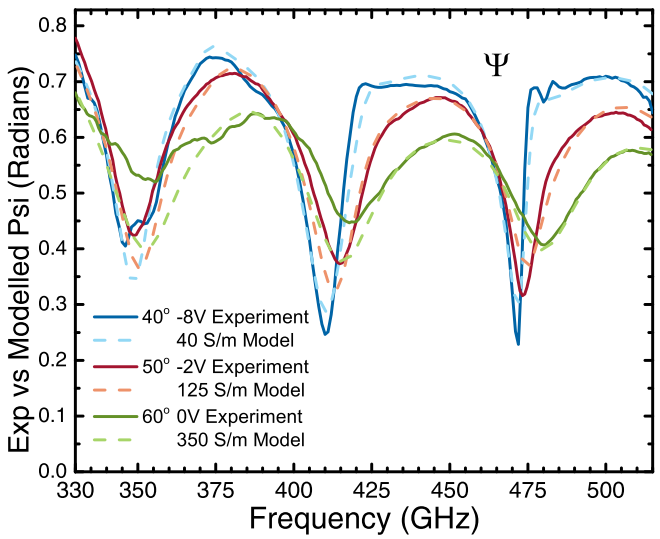

FIG. 3. Comparison between experimental and best-fit modelled data for the ellipsometric parameter Ψ at 40°, 50°, and 60° at different DC reverse voltage biases, showing the extent of the range of data used in the fitting procedure. The level of agreement between the measured and modeled values for the phase parameter Δ (not shown) is similar.

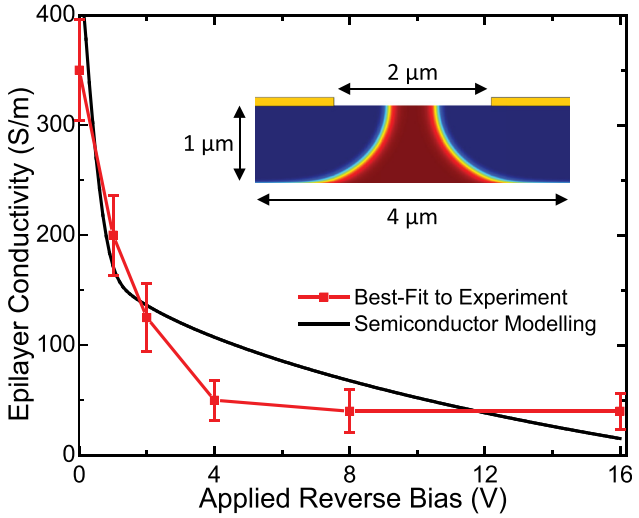

FIG. 4. Relation between the best-fit modelled epilayer conductivity value for each value of applied bias (red data points). The epilayer conductivity drops quickly and saturates with increasing voltage. The error bars represent the standard deviation of the best fit. The black curve shows a simulation of the gap region in the eSRR unit cell, showing how the averaged epilayer conductivity drops when a reverse bias is applied. The inset shows the simulated conductivity vs. position in the epilayer with an 8 V reverse voltage bias applied to the Schottky contacts (shown in yellow).

reasonable agreement with earlier estimates on a similar structure.[24] To further validate these results, we compare with semiconductor DC field simulations, using the finite volume method, of an ideal Schottky barrier diode in a cross-section centered on the eSRR split gap. From this simulation, we obtain the spatially averaged DC conductivity, $\sigma = N_D \mu_n e$, within the top 0.5 μm of the epilayer. This simulated trend with voltage is in reasonable agreement with the conductivity values obtained from the ellipsometry experiments, further confirming the plausibility of our results. The slight disagreement could result from the spatial averaging, which neglects the continuous variation in carrier density near the metal contact.

Using Fig. 4, we can now predict the behavior of this active metasurface in different configurations. One geometry of particular interest is to use the GaAs substrate as a planar dielectric slab waveguide[19] with the active 2D metasurface forming one boundary between the dielectric and air. This configuration is similar to previous studies of surface waves on THz metasurfaces,[16,17] but unlike in earlier measurements, our meta-elements are switchable, and our primary focus is on the possibility of active phase modulation of the guided wave.

A schematic of the experiment is illustrated in the inset of Fig. 5, showing the wafer illuminated in an end-fire configuration. To optimize the coupling efficiency from the free-space input beam, we use a metal parallel-plate waveguide (PPWG) to first form a well-defined TE_1 mode. This short section of PPWG (not shown in Fig. 5) is positioned directly adjacent to the edge of the metasurface slab, on-axis with the input beam. The plate separation of the PPWG is adjusted to be 50 μm larger than the thickness of the 650 μm GaAs slab. The initial edge of the wafer is not patterned with any metasurface, and so, we can directly excite the TE_1 mode of the slab waveguide with high efficiency. We estimate the

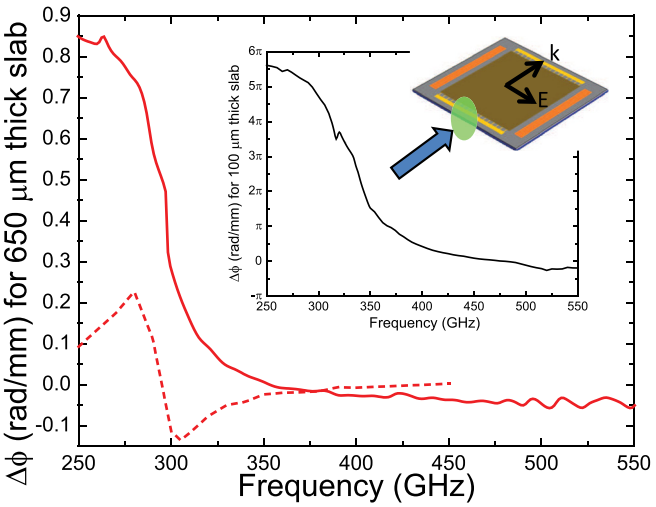

FIG. 5. Results of the phase modulation measured in the experimental slab waveguide (solid red curve), compared with the phase modulation predicted from the simulation (dashed red curve). Here, we plot the unwrapped phase modulation $\Delta\phi$ (as defined in the text) per mm of interaction with the metasurface. The qualitative agreement between the two red curves is acceptable, given the multi-mode nature of the propagation in this thick substrate. In the inset, we show the simulated result for a thin (100 μm) slab waveguide, where single-mode propagation is guaranteed up to ~450 GHz. Here, the phase modulation per mm is very large, especially at low frequencies. The cartoon inset shows a simplified illustration of the slab waveguide geometry. The metasurface device in Fig. 1 is face up with the THz input beam spot shown in green. Propagation direction in the slab waveguide mode is indicated by k. For TE modes, the electric field is in the plane of the metasurface, as shown.

mode-matching efficiency by computing the spatial overlap between the TE_1 PPWG mode and the lowest-order TE slab mode. This overlap is greater than 99%, and the coupling efficiency from the PPWG to the slab is calculated to be 62% due to reflection losses at the air-semiconductor boundary. With the given slab thickness, it operates as a single-mode waveguide only for frequencies up to 67 GHz; however, our mode-matching procedure efficiently excites only the lowest-order TE mode, even above the cutoff of higher-order modes.[25,26] Therefore, we can assume that the propagation remains single-mode in the slab, until the propagating mode reaches the region patterned by the metasurface. At this point, the mode experiences a voltage-dependent phase and amplitude response. This asymmetry in the waveguide disrupts the TE_1 mode, leading to coupling to higher-order TE-like hybrid modes.

We are especially interested in the phase modulation capabilities of this active waveguide, which occur as part of a coupled amplitude-phase modulation arising from the metamaterial response. We define this phase modulation $\Delta\phi$ as the difference in the total accumulated phase of the guided mode between the case when the metasurface has no DC bias applied and the case when there is a 6 V DC reverse bias applied to every element of the metasurface. The length of the slab waveguide containing meta-elements (eSRR elements) is 2.35 cm. In this distance, the propagating guided mode passes 224 rows of eSRR elements (and several connecting wires) as it traverses through the waveguide. Experimentally, we obtain $\Delta\phi$ by measuring a transmitted time-domain waveform at a fixed location outside of the waveguide in the two voltage configurations and comparing their spectral phases. A direct comparison with the simulation is impossible because the structure is far too large for a simulation of the entire propagation path. In addition, the eSRR structures on one surface of the slab induce multi-mode propagation in the thick slab as noted above, which makes a detailed analysis challenging. Nevertheless, we can obtain some information by simulating a smaller region of the waveguide (56 rows of eSRR elements, corresponding to a propagation length of 4.9 mm) and then assuming that $\Delta\phi$ accumulates linearly with the number of eSRR elements. In this case, we can scale the predicted value of $\Delta\phi$ to compare with the length used in the experiment. This comparison is shown in Fig. 5. We find rough agreement between the measured and simulated values of the 650 μm device, which displays a surprisingly large phase modulation in the low-frequency range of this measurement. As a suggestive comparison, we also show in the inset the simulated value of $\Delta\phi$ for a thinner dielectric slab waveguide (100 μm), with the same switchable metasurface on one face. The thinner slab is advantageous because it supports only a single TE mode to 447 GHz, and the propagation remains single-mode (and dominantly TE) even when the wave is in the asymmetric region of the waveguide (with a metasurface on just one boundary). As a result, the phase modulation results are more readily extracted from the simulation. In addition, thinning the slab reduces the mode confinement, resulting in an enhanced overlap between the guided wave and the metasurface. Our calculations predict a giant phase modulation at the metasurface resonance frequency, exceeding 2π per 8 eSRR elements, corresponding to only 700 μm of interaction length. The possibility of achieving 2π phase modulation in such a short structure holds great promise for device applications, as it will minimize the insertion loss of the device.

In conclusion, we have used THz ellipsometry to characterize the active response of an electrically tunable metasurface device, where the applied voltage is modelled as a tuning of the epilayer conductivity. Using these results, we predict the performance of the device in a slab waveguide configuration and compare with experimental results. We observe a phase modulation with a remarkably large magnitude of, e.g., 0.4 rad/mm of propagation at 300 GHz, which can be switched using a DC voltage. Moreover, we propose a waveguide geometry in which a modulation exceeding 2π/mm can be achieved for radiation with a free-space wavelength between 0.88 and 1.2 mm. This will enable full phase control of THz signals in this spectral range as well as versatile engineering of THz wavefronts.

This work was performed, in part, at the Center for Integrated Nanotechnologies, an Office of Science User Facility operated for the U.S. Department of Energy (DOE), Office of Science by Los Alamos and Sandia National Laboratories. Sandia National Laboratories is a multimission laboratory managed and operated by National Technology and Engineering Solutions of Sandia, LLC., a wholly owned subsidiary of Honeywell International, Inc., for the U.S. Department of Energy's National Nuclear Security Administration under Contract No. DE-NA-0003525. Los Alamos National Laboratory is operated by Los Alamos National Security, LLC, for the National Nuclear Security Administration of the U.S. Department of

Energy under Contract NO. DE-AC52-06NA25396. We also acknowledge funding support from the Army Research Office and the National Science Foundation.

[1]T. Kürner and S. Priebe, J. Infrared Millimeter, Terahertz Waves **35**, 53 (2014).
[2]T. Nagatsuma, G. Ducournau, and C. C. Renaud, Nat. Photonics **10**, 371 (2016).
[3]S. Jia, X. Yu, H. Hu, J. Yu, P. Guan, F. D. Ros, M. Galili, T. Morioka, and L. K. Oxenløwe, Opt. Express **24**, 23777 (2016).
[4]K. Sengupta and A. Hajimiri, IEEE J. Solid-State Circuits **47**, 3013 (2012).
[5]R. Kersting, G. Strasser, and K. Unterrainer, Electron. Lett. **36**, 1156 (2000).
[6]C.-Y. Chen, C.-F. Hsieh, Y.-F. Lin, R.-P. Pan, and C.-L. Pan, Opt. Express **12**, 2625 (2004).
[7]Z. Miao, Q. Wu, X. Li, Q. He, K. Ding, Z. An, Y. Zhang, and L. Zhou, Phys. Rev. X **5**, 041027 (2015).
[8]H.-T. Chen, W. J. Padilla, M. J. Cich, A. K. Azad, R. D. Averitt, and A. J. Taylor, Nat. Photonics **3**, 148 (2009).
[9]Y. Zhang, S. Qiao, S. Liang, Z. Wu, Z. Yang, Z. Feng, H. Sun, Y. Zhou, L. Sun, Z. Chen *et al.*, Nano Lett. **15**, 3501 (2015).
[10]S. Rout and S. R. Sonkusale, APL Photonics **1**, 086102 (2016).
[11]H.-T. Chen, W. J. Padilla, J. M. Zide, A. C. Gossard, A. J. Taylor, and R. D. Averitt, Nature **444**, 597 (2006).
[12]W. L. Chan, H.-T. Chen, A. J. Taylor, I. Brener, M. J. Cich, and D. M. Mittleman, Appl. Phys. Lett. **94**, 213511 (2009).
[13]N. Karl, K. Reichel, H.-T. Chen, A. J. Taylor, I. Brener, A. Benz, J. L. Reno, R. Mendis, and D. M. Mittleman, Appl. Phys. Lett. **104**, 091115 (2014).
[14]C. M. Watts, D. Shrekenhamer, J. Montoya, G. Lipworth, J. Hunt, T. Sleasman, S. Krishna, D. R. Smith, and W. J. Padilla, Nat. Photonics **8**, 605 (2014).
[15]H.-T. Chen, A. J. Taylor, and N. Yu, Rep. Prog. Phys. **79**, 076401 (2016).
[16]B. Reinhard, O. Paul, R. Beigang, and M. Rahm, Opt. Lett. **35**, 1320 (2010).
[17]M. F. Volk, B. Reinhard, J. New, R. Beigang, and M. Rahm, Opt. Lett. **38**, 2156 (2013).
[18]S. Maci, G. Minatti, M. Casaletti, and M. Bosiljevac, IEEE Antennas Wireless Propag. Lett. **10**, 1499 (2011).
[19]R. Mendis and D. Grischkowsky, J. Appl. Phys. **88**, 4449 (2000).
[20]J. P. Turpin, J. A. Bossard, K. L. Morgan, D. H. Werner, and P. L. Werner, Int. J. Antennas Propag. **2014**, 429837.
[21]T. Hofmann, C. M. Herzinger, A. Boosalis, T. E. Tiwald, J. A. Woollam, and M. Schubert, Rev. Sci. Instrum. **81**, 023101 (2010).
[22]M. Neshat and N. P. Armitage, J. Infrared Millimeter, Terahertz Waves **34**, 682 (2013).
[23]*Handbook of Ellipsometry* edited by H. G. Tompkins and E. A. Irene (William Andrews Publishing, Norwich, NY, 2005).
[24]K. Fan, H. Y. Hwang, M. Liu, A. C. Strikwerda, A. Sternbach, J. Zhang, X. Zhao, X. Zhang, K. A. Nelson, and R. D. Averitt, Phys. Rev. Lett. **110**, 217404 (2013).
[25]R. Mendis and D. M. Mittleman, J. Opt. Soc. Am. B **26**, A6 (2009).
[26]M. Mbonye, R. Mendis, and D. M. Mittleman, Opt. Express **20**, 27800 (2012).